Energy Conversion and Management 195 (2019) 99–113

Contents lists available at ScienceDirect

Energy Conversion and Management

journal homepage: www.elsevier.com/locate/enconman

Overlap energy utilization reaches maximum efficiency for S-CO_2 coal fired power plant: A new principle

Enhui Sun[a], Jinliang Xu[a,b,*], Han Hu[a], Mingjia Li[c], Zheng Miao[a], Yongping Yang[b], Jizhen Liu[b]

[a] Beijing Key Laboratory of Multiphase Flow and Heat Transfer for Low Grade Energy Utilization, North China Electric Power University, Beijing 102206, China
[b] Key Laboratory of Condition Monitoring and Control for Power Plant Equipment of Ministry of Education, North China Electric Power University, Beijing 102206, China
[c] Key Laboratory of Thermo-Fluid Science and Engineering of Ministry of Education, School of Energy & Power Engineering, Xi'an Jiaotong University, Xi'an, Shaanxi 710049, China

ARTICLE INFO

Keywords:
Overlap energy utilization
Supercritical carbon dioxide
Thermal efficiency
Top cycle
Bottom cycle

ABSTRACT

For a coal fired power plant, a combined supercritical CO_2 cycle (S-CO_2) absorbs flue gas energy over entire temperature range. Because top/bottom cycles absorb high and moderate temperature flue gas energy respectively, there is an efficiency gap between the two cycles. To fill the efficiency gap, the overlap absorption of flue gas energy is proposed, using top cycle to absorb high temperature flue gas heat, but bottom cycle to absorb not only moderate temperature flue gas heat, but also a part of high temperature flue gas heat. The overlap energy absorption in a high temperature regime increases CO_2 heat absorption temperature to improve bottom cycle efficiency. A four steps roadmap guides us to construct a combined cycle with RC + DRH as top cycle and RC + DRH + EAP as bottom cycle to reach the maximum efficiency limit, where RC, DRH and EAP represent the cycles of recompression, double-reheating and external air preheater, respectively. The components sharing among top/bottom cycles ensures simple system layout, and EAP recycles extra heat of bottom cycle to the system, keeping a smallest heat dissipation to environment. The net power efficiency reaches 47.99% at the main vapor parameters of 620 °C/30 MPa. The overlap energy utilization can be extended for other systems.

1. Introduction

Water has been used as the working fluid in thermal cycles to convert thermal energy into power for more than one century [1]. Water-steam based Rankine cycle is widely applied by most of commercial power plants driven by fossil energy of coal or natural gas, nuclear energy or solar energy [2–5]. Even though the turbine inlet pressure is sufficiently high, some facilities such as condenser still operate in vacuum pressure to significantly enlarge the whole power plant design [6]. Besides, a high temperature (~700 °C) water-steam reacts with metallic materials, limiting further increment of turbine inlet vapor temperature to improve the cycle efficiency [7,8].

Supercritical carbon dioxide Brayton (S-CO_2) cycle was first proposed by Sulzer [9] and analyzed by Feher [10]. Benefits of S-CO_2 cycle are: (1) at a main vapor temperature higher than 550 °C, thermal efficiency can be higher than a water-steam Rankine cycle [11]; (2) CO_2 is an inert fluid to weaken the chemical reaction with metallic materials [12]; and (3) S-CO_2 cycle is compact due to the whole system operating in supercritical pressures [13]. Recent progresses have been made on the development of S-CO_2 cycle driven by nuclear energy or solar energy [14–17].

Fossil energy based thermal power plants face new challenges in high efficiency, ultra-low emission and compact size [18–20]. Especially, renewable energy (wind or solar) is being expanded to generate electricity. When renewable energy is connected with a power grid, the power grid becomes fragile [21]. An effective way to create robust power grid is to develop hybrid power system consisting of both renewable energy and coal fired power plant [22]. The coal fired power plant should be sensitive enough to adapt the quick load variation of renewable energy. A water-steam Rankine cycle is difficult to satisfy this requirement, but S-CO_2 cycle has the potential to achieve this requirement due to compact system [13,23,24].

The development of S-CO_2 coal fired power plant is in infancy stage [25–28]. Xu et al. [25] commented key issues and solution strategies for S-CO_2 coal fired power plant. A S-CO_2 boiler converts coal chemical energy into thermal energy of flue gas, heating CO_2 fluid in boiler tubes. The generated vapor drives turbines for power generation. The coupling between S-CO_2 boiler and S-CO_2 cycle is a challenge issue. Usually, the boiler flue gas covers a very wide temperature range. For example, the flame temperature can be ~1500 °C, but the exit flue gas temperature is limited by a low value such as 120 °C. A single S-CO_2 cycle cannot

* Corresponding author.
E-mail address: xjl@ncepu.edu.cn (J. Xu).

https://doi.org/10.1016/j.enconman.2019.05.009
Received 25 February 2019; Received in revised form 30 April 2019; Accepted 2 May 2019

Nomenclature

b	bottom cycle
C	compressor
CTB	connected-top-bottom
CTBO	connected-top-bottom cycle with overlap utilization
DRH	double reheat
EAP	external air preheater
h	specific enthalpy
HTC	high temperature cooler
HTR	high temperature recuperator
l	length of tube
LTR	low temperature recuperator
m	mass flow rate
P	pressure
Q	heat transfer load
RC	recompression cycle
RH	reheater
SH	superheater
S-CO_2	supercritical carbon dioxide
t	top cycle
T	turbine
T	temperature

Subscripts

1, 2, 3…	state points of top cycle
1b, 2b, 3b…	state points of bottom cycle
a	absorb
AP	air preheater
ave	average
e	environment
ex	exhaust
fg	flue gas
i	in
H	high temperature regime
M	moderate temperature regime
o	out
r	release
s	isentropic
sec	secondary

Greek symbols

β	the ratio of Q_b to Q_t
δ	deviation temperature
ΔT_p	pinch temperature difference
η_b	boiler efficiency
η_e	power efficiency
η_g	power generator efficiency
η_p	pipeline efficiency
$\eta_{th,b}$	bottom cycle thermal efficiency
$\eta_{th,s}$	whole system thermal efficiency
$\eta_{th,t}$	top cycle thermal efficiency

absorb flue gas heat over an entire temperature range. Recently, Sun et al. [26] proposed a method to cascade utilize the flue gas heat. Flue gas energies in high, moderate and low temperature levels are extracted by a top S-CO_2 cycle, a bottom S-CO_2 cycle, and an air preheater, respectively. The three temperature regimes are consecutively arranged in a temperature decrease direction, satisfying the cascade energy utilization principle. Because some components such as coolers and recuperator heat exchangers may have similar pressure/temperature values for top and bottom cycles, these components are suggested to be shared and combined among the two cycles, significantly simplifying the whole cycle layout.

For cascade utilization of flue gas heat, because top and bottom cycles are heated by flue gas in different temperature levels, the CO_2 vapor temperature at turbine inlet is different for the two cycles. It's known that thermal efficiency of a cycle depends on turbine inlet temperature (the maximum fluid temperature in the cycle). Thus, cascade energy utilization yields an efficiency difference between top and bottom cycles. The bottom cycle efficiency is lower than the top cycle. For large scale power plant, a small increment of power generation efficiency η_e results in an obvious energy saving. For example, for a 1000 MWe power plant, when η_e is increased from 47% to 48%, about 6.8 tons of standard coal can be saved per hour. The sensitive efficiency to energy saving inspired us to explore new idea to further increase the system efficiency. The raised questions are: is it possible to have the same thermal efficiencies of the top and bottom cycles? Where is the maximum efficiency limit for the whole power plant?

In order to fill the efficiency gap between top and bottom cycles, the overlap energy utilization is proposed in this paper. The entire flue gas energy is classified into a high temperature regime, a moderate temperature regime and a low temperature regime. Different from cascade energy utilization, an overlap sub-regime is set in high temperature regime, under which a top cycle absorbs a major part (not all) of high temperature flue gas heat, a bottom cycle absorbs not only moderate temperature flue gas heat, but also a small percentage of high temperature flue gas heat, and an air preheater receives low temperature flue gas heat. Thus, the overlap energy utilization is defined, so that bottom cycle can have higher CO_2 temperature for power generation. Because top cycle has the largest thermal efficiency, this efficiency is taken as the reference and target value for bottom cycle and combined cycle of the whole system. For S-CO_2 cycle, the thermal efficiency is scaled as $1-T_{ave,r}/T_{ave,a}$, where $T_{ave,a}$ is the average heat absorption temperature, and $T_{ave,r}$ is the average heat release temperature. Such definitions are made for both top and bottom cycles. Maximum system efficiency is reached when both top and bottom cycles have same $T_{ave,a}$ and $T_{ave,r}$. Four steps roadmap guides us to reach this target. The analysis is started from the cascade energy utilization using RC + DRH as top cycle and RC as bottom cycle (case A). Cases B, C and D for overlap energy utilization gradually approach the final target.

The present paper is organized as follows. Fundamental consideration of overlap energy utilization is described in Section 2 (see Fig. 1). Numerical model for cycle computation is dealt with in Section 3 (see Fig. 2). Section 4 reports results and discussion, in which sub-section 4.1 deals with case A including Figs. 3–5, sub-section 4.2 deals with case B including Figs. 6–8, sub-section 4.3 deals with case C including Figs. 9–11, and Section 4.4 deals with case D including Figs. 12–18. Section 5 comments on the overlap energy utilization. Major conclusions are summarized in Section 6.

2. Overlap energy utilization principle

Fig. 1a describes cascade utilization of flue gas heat. In flue gas side, the three regimes are marked as 1500 °C-$T_{fg,i}$, $T_{fg,i}$-$T_{fg,o}$, and $T_{fg,o}$-$T_{fg,ex}$,

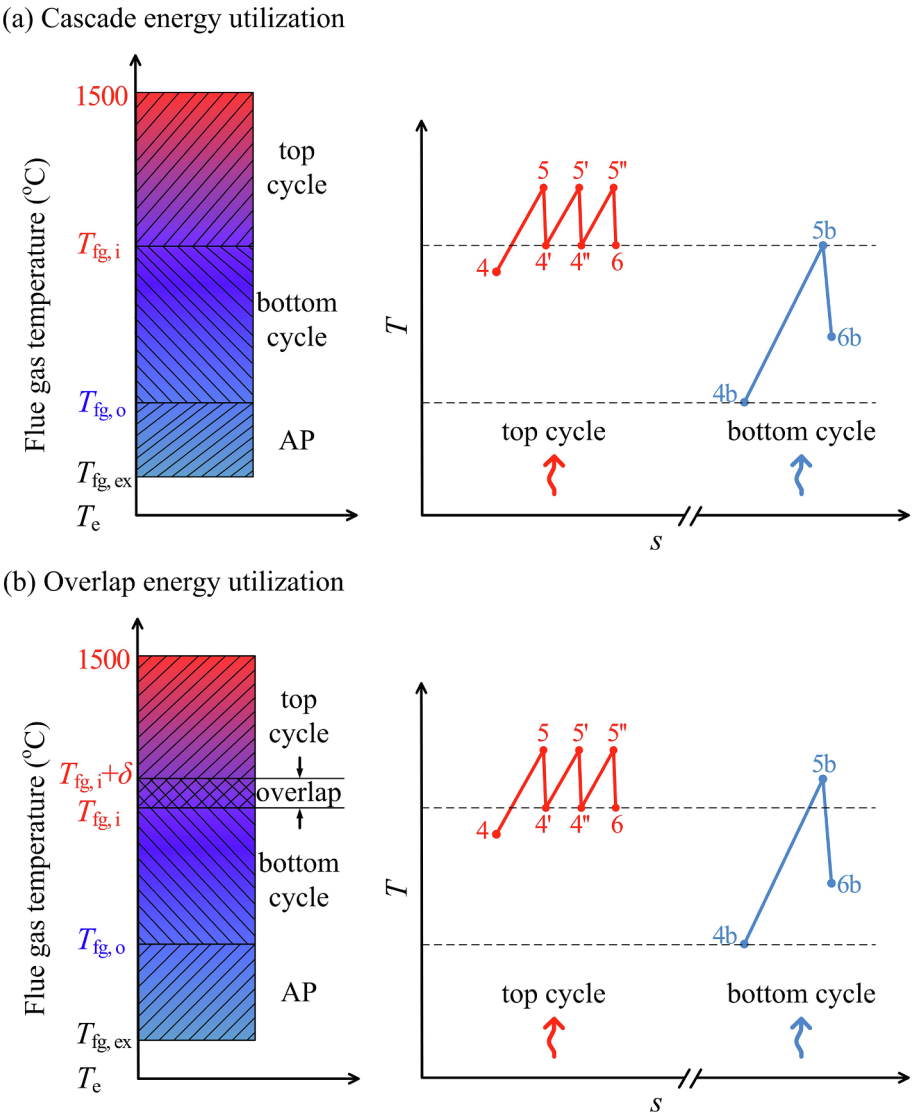

Fig. 1. Two energy utilization principles (a: cascade energy utilization, b: overlap energy utilization).

where ~1500 °C is the flame temperature, $T_{fg,i}$ is the interface temperature between high and moderate temperature regimes, $T_{fg,o}$ is the interface temperature between moderate and low temperature regimes, $T_{fg,ex}$ is the exit flue gas temperature. *T-s* diagrams are qualitatively plotted in Fig. 1a for heating and expansion processes, where *T* and *s* are the temperature and entropy, respectively. For top cycle, multi-heating processes are marked as 45, 4′5′ and 4″5″, while multi-expansion processes are marked as 54′, 5′4″ and 5″6. For bottom cycle, heating and expansion processes are marked as 4b5b and 5b6b, respectively, where *b* means bottom cycle. For both flue gas side and CO_2 fluid side, the temperatures are consecutively arranged. The cascade energy utilization satisfies the criterion of $T_{5b} = T_{4'}$.

For a heat engine working in a temperature difference between T_a (isothermal heat source) and T_r (isothermal heat sink), the Carnot efficiency is

$$\eta_{th} = 1 - \frac{T_r}{T_a} \tag{1}$$

For heating and cooling processes with varied temperature roadmaps, Eq. (1) is modified as

$$\eta_{th} \approx 1 - \frac{T_{ave,r}}{T_{ave,a}} \tag{2}$$

where $T_{ave,a}$ and $T_{ave,r}$ are determined by [29,30]

$$T_{ave,a} = \frac{\sum_{i=1}^{N} Q_{h,i}}{\sum_{i=1}^{N} \Delta S_{h,i}} = \frac{\sum_{i=1}^{N} m_i (h_{h,out,i} - h_{h,in,i})}{\sum_{i=1}^{N} m_i \Delta s_{h,i}} \tag{3}$$

$$T_{ave,r} = \frac{\sum_{i=1}^{M} Q_{c,i}}{\sum_{i=1}^{M} \Delta S_{c,i}} = \frac{\sum_{i=1}^{M} m_i (h_{c,out,i} - h_{c,in,i})}{\sum_{i=1}^{M} m_i \Delta s_{c,i}} \tag{4}$$

In Eqs. (3) and (4), *Q* is the heat transfer load, *m* is the mass flow rate of cycling fluid, *i* means the *i*th heating or cooling process, for example, 45 is a heating process ($i = 1$), 4′5′ is another heating process ($i = 2$), *N* and *M* are the number of heating and cooling process, respectively, the subscript *in* and *out* represent inlet and outlet states for

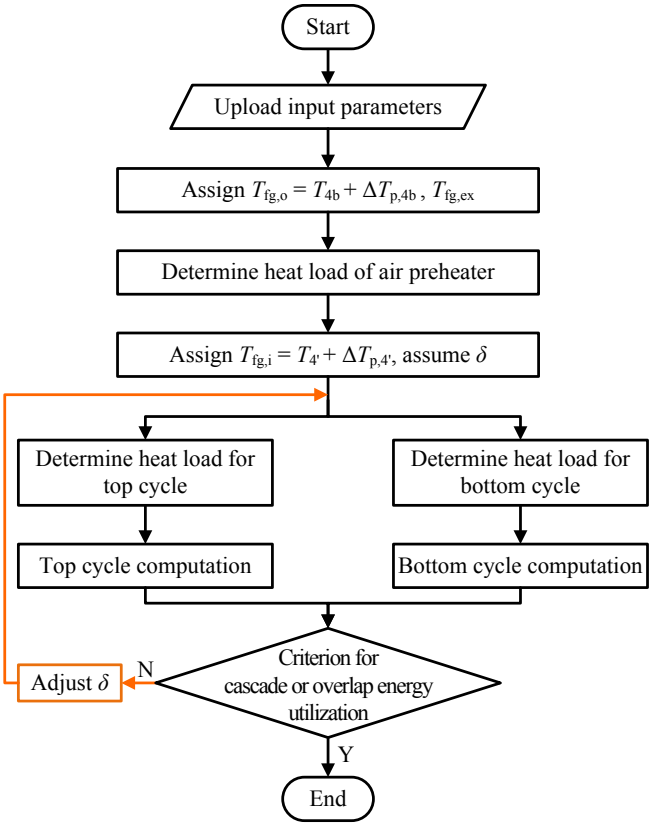

Fig. 2. Logic framework of the computation process for cascade/overlap energy utilization for S-CO_2 coal fired power plant.

i[th] process, the subscripts h and c mean heating process and cooling process, respectively. For cascade energy utilization, T_{5b} (maximum cycling fluid temperature for bottom cycle) equals to $T_{4'}$ (minimum cycling fluid temperature in tail flue for top cycle). Thus, $T_{ave,a}$ for bottom cycle is lower than that for top cycle to yield an efficiency gap between the two cycles.

Alternatively, Fig. 1b shows our newly proposed overlap energy utilization. In high temperature flue gas regime, an overlap sub-regime is set, covering a temperature range from $T_{fg,i} + \delta$ to $T_{fg,i}$, where δ is a deviation temperature. The flue gas heat in overlap regime is not only absorbed by top cycle, but also by bottom cycle. In cycling fluid side, the overlap heating obviously elevates T_{5b} ($T_{5b} > T_4$), making bottom cycle efficiency to approach top cycle efficiency. Meanwhile, a suitable (not too high) T_{4b} is maintained to absorb moderate temperature flue gas heat in the tail flue. Here, the overlap heating concept is proposed in a general sense. The cycling fluid can be supercritical CO_2 such as encountered in this paper, or water-steam for other cycles. In Section 4, the roadmap from case A to case D guides us to equalize the thermal efficiencies between top cycle and bottom cycle by using the overlap heating principle. Identical efficiencies of top and bottom cycles change the conventional cognition that "*bottom cycle efficiency is lower than top cycle, because the bottom cycle operates in a lower temperature level*".

The same efficiencies of the two cycles is easy to be understood. One shall remember that the temperature difference between flame (flue gas) and cycling fluid is sufficiently high. Assuming a flame temperature of ~1500 °C and a maximum cycling fluid temperature of 600–700 °C, the temperature difference is up to 800–900 °C. Cascade energy utilization causes ultra-large exergy destruction in heat transfer process between flue gas in "furnace" and cycling fluid in "boiler". On the contrary, the overlap heating deeply uses the available exergy of high temperature flue gas. In other words, high temperature flue gas has sufficient capability to elevate the cycling fluid temperature for bottom cycle in a similar level as to that for top cycle.

3. Numerical model

3.1. Cascade/overlap energy utilization

In this paper, the input parameters are specified by a 1000 MWe coal fired power plant. Fig. 2 shows the calculation logic. Both cascade and overlap heating involve the flue gas energy distribution in three temperature regimes. This distribution is coupled with top and bottom S-CO_2 cycles (see Figs. 1 and 2). The low temperature flue gas heat absorbed by air preheater is determined first. $T_{fg,o}$ is the flue gas temperature entering air preheater:

$$T_{fg,o} = T_{4b} + \Delta T_{p,4b} \tag{5}$$

where T_{4b} is the boiler inlet temperature of bottom cycle, $\Delta T_{p,4b}$ is the pinch temperature difference in Heater 4. $\Delta T_{p,4b} = 30$ °C is applied in this study. Once an exit flue gas temperature $T_{fg,ex}$ is given ($T_{fg,ex} = 123$ °C), the heat load assigned to air preheater is

$$Q_{AP} = m_{gas}(h_{T_{fg,o}} - h_{T_{fg,ex}}) \tag{6}$$

where m_{gas} is the mass flow rate of flue gas, h is the flue gas enthalpy determined at the two interface temperatures of $T_{fg,o}$ and $T_{fg,ex}$.

Then, heat loads assigned to top cycle and bottom cycle are to be determined. This determination depends on the interface temperature $T_{fg,i}$, which equals $T_{4'}$ plus $\Delta T_{p,4'}$ ($\Delta T_{p,4'} = 40$ °C here). The flue gas energy in high temperature regime $Q_{gas,H}$ and moderate temperature regime $Q_{gas,M}$ are

$$Q_{gas,H} = m_{gas}(h_{T_{flame}} - h_{T_{fg,i}}), \quad Q_{gas,M} = m_{gas}(h_{T_{fg,i}} - h_{T_{fg,o}}) \tag{7}$$

where T_{flame} is the highest flue gas temperature in furnace such as ~ 1500 °C set in this paper.

For cascade energy utilization, $\delta = 0$ is used. For overlap heating, a specific δ is assumed, in which the flue gas heat is absorbed by both top and bottom cycles. The top cycle absorbs the major part of high temperature flue gas heat (not all). The bottom cycle absorbs flue gas heat across both high and moderate temperature regimes. After the heat load assignment is complete, thermodynamics coupling with thermal-hydraulic characteristic for top and bottom cycles is considered. The above process is iterated to verify if the energy utilization criterion is satisfied (see Figs. 1 and 2):

$$\begin{cases} T_{5b} = T_{4'} & \leftarrow \text{cascade energy use} \\ T_{5b} = T_5 = T_{5'} = T_{5''} & \leftarrow \text{overlap energy use} \end{cases} \tag{8}$$

The cascade energy utilization criterion is that "*CO_2 temperature entering turbine for bottom cycle equals to CO_2 temperature entering boiler for top cycle*", while the overlap energy utilization ensures "*identical CO_2 temperature entering each turbine for both top and bottom cycles*". The computation process is stopped if Eq. (8) is satisfied, otherwise, δ is adjusted to repeat the above calculation.

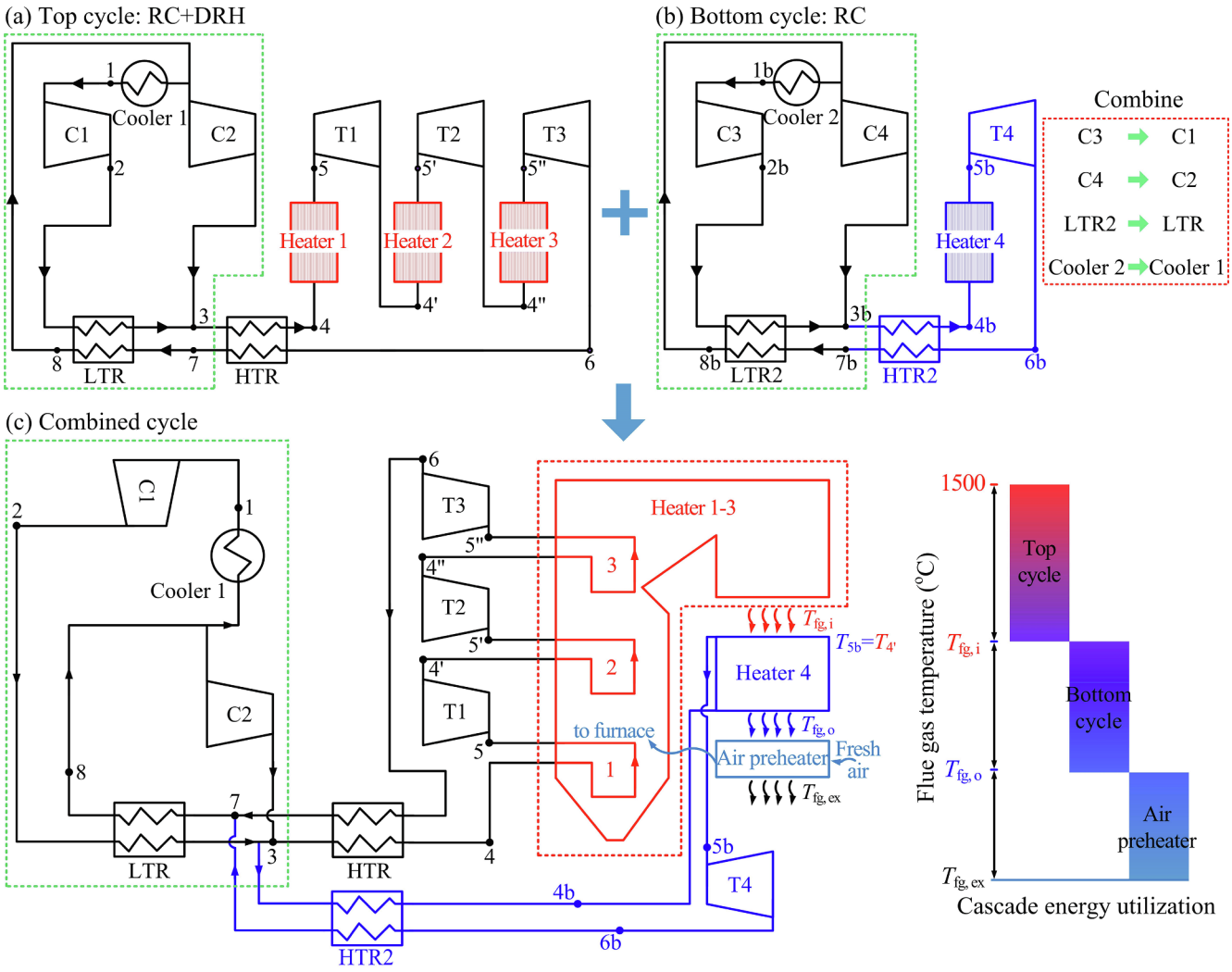

Fig. 3. Case A: CTB (RC + DRH + RC) with cascade absorption of flue gas heat (a: top cycle, b: bottom cycle, c: combined cycle with components sharing).

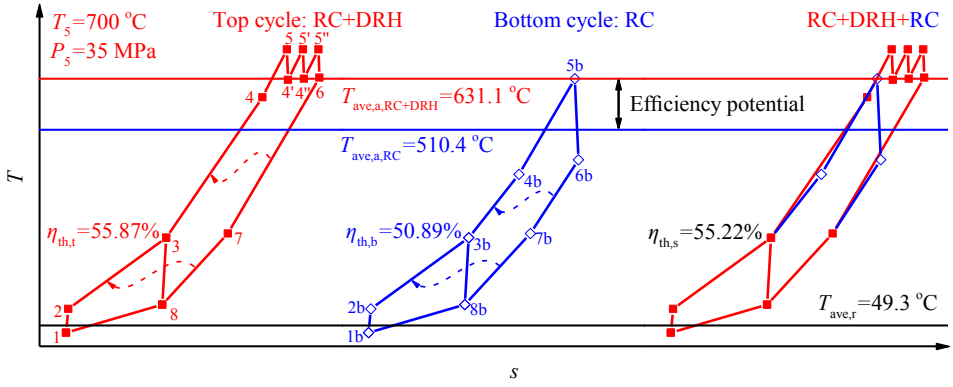

Fig. 4. *T-s* diagram for CTB (RC + DRH + RC) with cascade absorption of flue gas heat ($T_{5b} = T_{4'}$).

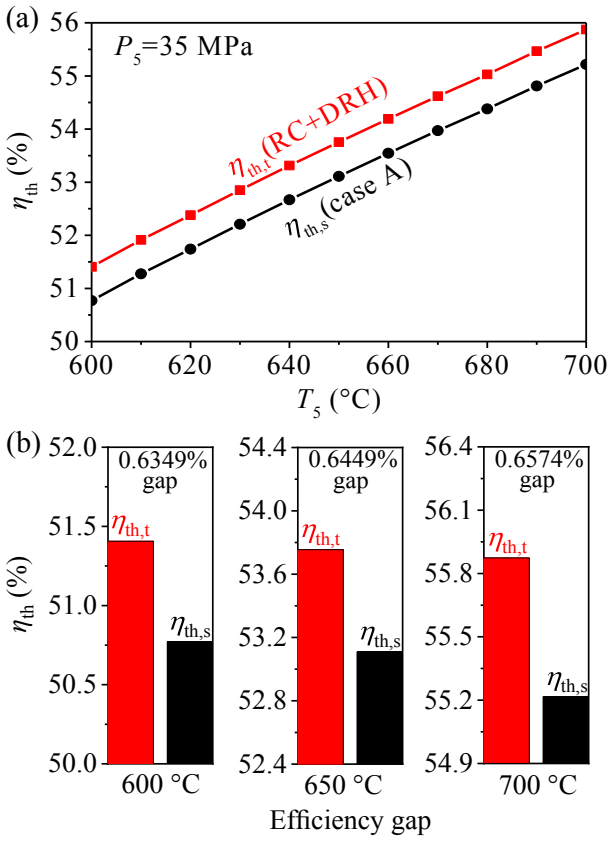

Fig. 5. Thermal efficiencies of CTB (RC + DRH + RC) referenced to top cycle (RC + DRH) (a: efficiencies versus main vapor temperatures for top cycle and combined cycle, b: efficiency gaps between top cycle and combined cycle at three main vapor temperatures).

3.2. Thermodynamics cycle coupled with boiler thermal-hydraulic characteristic

In the present study, the top cycle always uses RC + DRH, which is believed to have better efficiency compared with other cycles [25,28], but the bottom cycle either uses RC, or RC + DRH. Let's introduce recompression cycle (RC) first, see bottom cycle in Fig. 3. The total mass flow rate of CO_2 at the outlet of LTR2 (low temperature recuperator heat exchanger) (state 8b) is split into two streams, with one stream being pressurized by compressor C4, the other stream is cooled by cooler 2 (heat dissipation to environment), pressurized by compressor C3 and then enters the inlet of LTR2. Then the two streams mix at point 3 and enter the inlet of HTR2 (high temperature recuperator heat exchanger). The entire mass flow rate is heated by Heater 4 and drives turbine T4. In contrast to RC with one heater and one turbine only, RC + DRH, where DRH means double-reheating, has three heaters and three turbines (see top cycle in Fig. 3).

The thermodynamic computation links various components together by pressure/temperature parameters at various state points. The calculation should be performed for each component. For example, turbine T4 in bottom cycle of Fig. 3 writes

$$\eta_{T4,s} = \frac{h_{5b} - h_{6b}}{h_{5b} - h_{6b,s}}, \quad w_{T4} = h_{5b} - h_{6b} \tag{9}$$

where $\eta_{T4,s}$ is the isentropic efficiency for turbine T4, h is the CO_2 enthalpy, $h_{6b,s}$ is the enthalpy based on isentropic expansion, and w_{T4} is the turbine power output per unit mass flow rate. The thermodynamic computation for other components can be referenced to [26,31], and not repeated here for simplification.

The thermodynamics analysis should couple the thermal-hydraulic characteristic of S-CO_2 boiler. The CO_2 mass flow rate is 6–8 times of that of a water-steam Rankine cycle, significantly raising boiler pressure drop to deteriorate the cycle efficiency [25]. In order to overcome this difficulty, Xu et al. [25] proposed the partial flow strategy and boiler module design. Fundamentally, considering a tube having a length l and a mass flow rate m (total flow mode), if the tube is segmented into two parallel and connected sections (partial flow mode), each having a length $0.5\,l$ and a mass flow rate $0.5\,m$, the frictional pressure drop is reduced to 1/8 of that for total flow mode, noting that the total heat transfer area and mass flow rate is not changed for total flow mode and partial flow mode. The partial flow mode and boiler module design are incorporated into a 1000 MWe S-CO_2 power plant design [25], which are also applied in this paper to couple the thermal-hydraulic characteristic of boiler.

Thermal efficiency is defined as net power (turbine power subtracting compressor consumed power) divided by heat absorption of the cycle. For combined cycle system, three thermal efficiencies are involved for top cycle $\eta_{th,t}$, bottom cycle $\eta_{th,b}$ and whole system $\eta_{th,s}$, respectively. They have the following relationship:

$$\eta_{th,s} = \frac{\eta_{th,t} Q_t + \eta_{th,b} Q_b}{Q_t + Q_b} = \frac{\eta_{th,t} + \beta \eta_{th,b}}{1 + \beta} \tag{10}$$

where $\beta = Q_b/Q_t$ is the ratio of bottom cycle heat absorption Q_b to top cycle heat absorption Q_t, βcan be thought as the sensitivity factor of the bottom cycle efficiency to the whole system efficiency. The system power efficiency η_e relates to other efficiencies as follows:

$$\eta_e = \eta_{th} \eta_b \eta_p \eta_g \tag{11}$$

where η_b is the boiler efficiency, which is 94.3% at $T_{fg,ex}$ = 123 °C, η_p is the pipeline efficiency and η_g is the generator efficiency. For large scale power plant, η_p can be a constant of 99% [25,32], η_g can be a constant of 98.5% [27,33]. The isentropic efficiencies of turbines and compressors are involved in the thermodynamics calculation such as shown in Eq. (9). Tables 1–3 list important parameters for top cycle, bottom cycle and designed coal.

4. Results and discussion

4.1. Cascade energy utilization: Case A with CTB (RC + DRH + RC)

Figs. 3–5 show case A with CTB (RC + DRH + RC). Even though top cycle and bottom cycle operate in different temperature levels, some components (not all) still have the possibility to have similar pressure/temperature values across inlet and outlet of these components. The *parameter coordination principle* shares these components between the two cycles [26]. CO_2 fluids in the two cycles are connected with each other, thus CTB (connected-top-bottom) cycle is called. In Fig. 3, compressor C3 in bottom cycle is combined with compressor C1 in top cycle, compressor C4 in bottom cycle is combined with compressor C2 in top cycle, low temperature recuperator heat exchanger LTR2 in bottom cycle is combined with LTR in top cycle, and cooler 2 in bottom cycle is combined with cooler 1 in top cycle. Totally four components are cut.

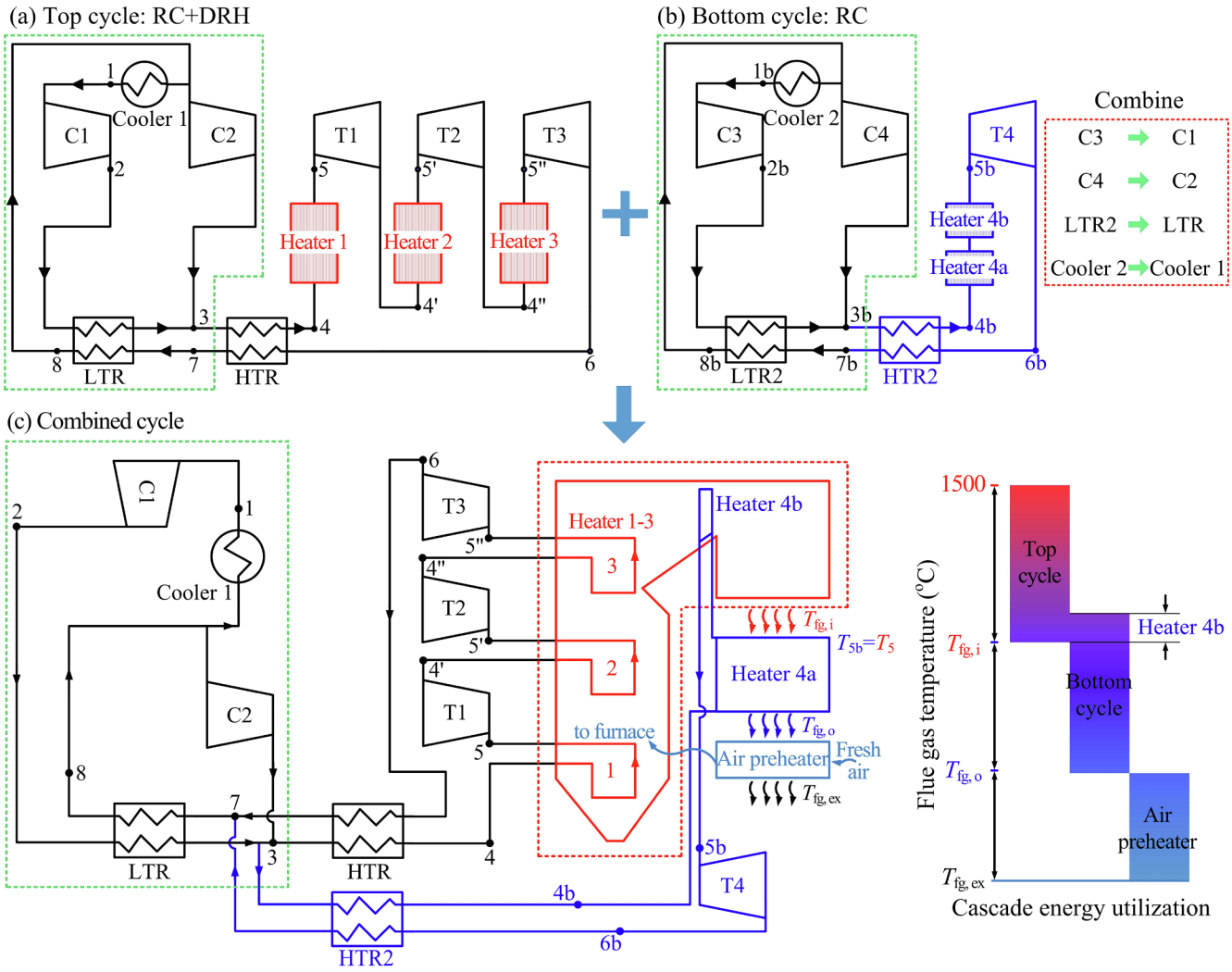

Fig. 6. Case B: CTBO (RC + DRH + RC) with overlap absorption of flue gas heat (a: top cycle, b: bottom cycle, c: combined cycle after components sharing).

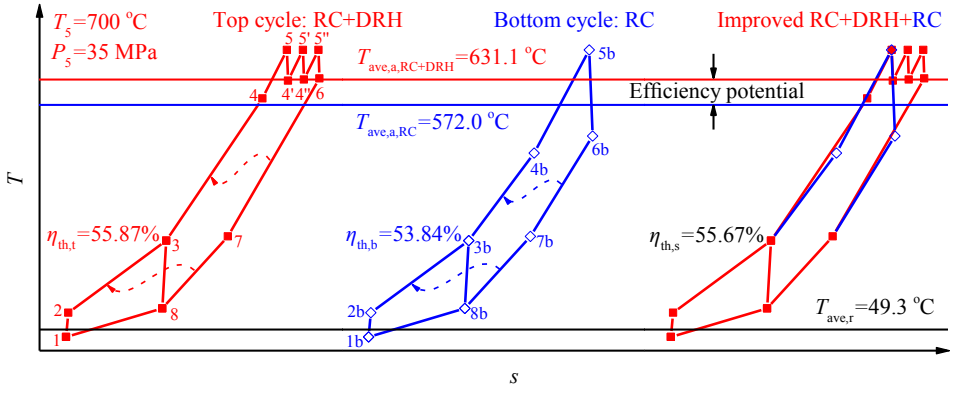

Fig. 7. *T-s* diagram for case B with CTBO (RC + DRH + RC): overlap absorption of flue gas heat with constraint of $T_{5b} = T_5 = T_{5'} = T_{5''}$.

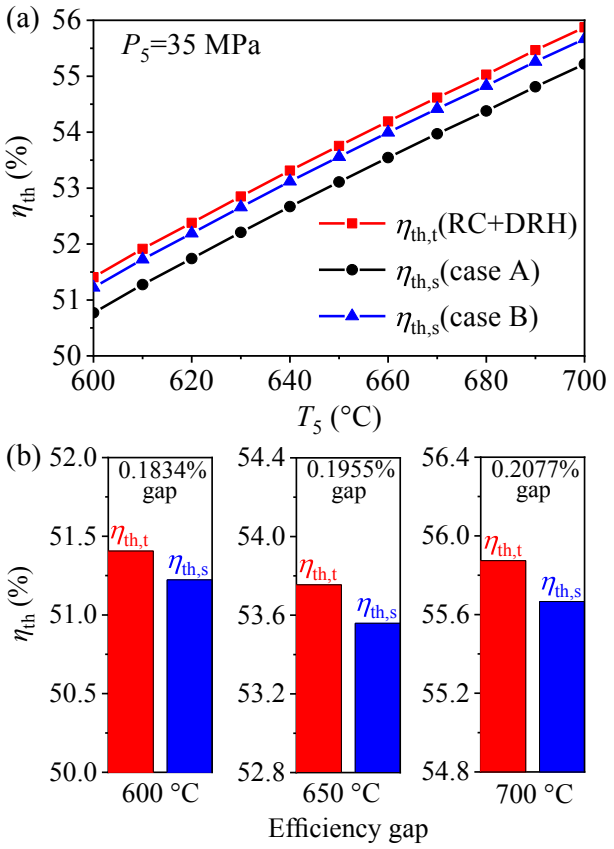

Fig. 8. Thermal efficiencies referenced to top cycle (a: thermal efficiencies of CTB (RC + DRH + RC) and CTBO (RC + DRH + RC) versus main vapor temperatures, b: efficiency gaps between top cycle and CTBO (RC + DRH + RC) at three main vapor temperatures).

Figs. 3–5 show that indeed, the temperature levels are consecutively arranged without overlap, in both flue gas side and CO_2 side. At the main vapor parameter of T_5 = 700 °C and P_5 = 35 MPa, top cycle and bottom cycle have the same average heat release temperature of 49.3 °C. However, the average heat absorption temperature $T_{ave,a}$ is 631.1 °C for top cycle, and 510.4 °C for bottom cycle. Correspondingly, thermal efficiency is 55.87% for top cycle and 50.89% for bottom cycle (see Fig. 4). The efficiency gap between the two cycles is obvious. One maybe interest in the efficiency gap between top cycle and whole system, which are represented by red ($\eta_{th,t}$) and black ($\eta_{th,s}$) colors respectively (see Fig. 5). Both efficiencies are linearly correlated with main vapor temperatures T_5. Covering T_5 in the range of 600–700 °C, the system efficiency $\eta_{th,s}$ is lower by 0.63%–0.66% than the top cycle $\eta_{th,t}$. This efficiency gap inspired us to apply the overlap energy utilization.

4.2. Overlap energy utilization: Case B with CTBO (RC + DRH + RC)

Figs. 6–8 show the connected-top-bottom cycle with overlap utilization of flue gas heat which is called CTBO. The cycles and components sharing are similar to Figs. 3–5 for cascade energy utilization. However, in order to heat CO_2 in an overlap regime, Heaters 4a and 4b are used instead of one. CO_2 in bottom cycle is initially heated by Heater 4a in moderate flue gas temperature regime, and further heated by Heater 4b in high temperature flue gas regime. Fig. 6 shows the overlap heating in flue gas side. Fig. 7 shows *T-s* diagram to indicate identical vapor temperatures entering turbine for bottom cycle and top cycle (T_{5b} = T_5) by overlap heating, which is impossible by cascade heating. For bottom cycle, the average heat absorption temperature $T_{ave,a}$ is increased from 510.4 °C by cascade heating to 572.0 °C by overlap heating to show obvious improvement. Fig. 8 shows that the overlap heating causes the combined cycle to approach the top cycle. The efficiency gap between top cycle and combined cycle becomes 0.18%-0.21%, which is significantly improved compared to cascade heating (see Fig. 5).

Case A indicates that, with main vapor temperatures T_5 in the range of 600–700 °C and primary air temperature of 320 °C, the secondary air temperatures $T_{sec\ air}$ are varied in the range of 291.8–396.4 °C, which is acceptable for practical application (Section 4.1). However, the overlap heating induced efficiency improvement accompanies a cost. With T_5 in the range of 600–700 °C, the secondary air temperatures are varied in the range of 361.3–473.9 °C, which is beyond the limit of 400 °C [34]. The mini efficiency gap and slight overheating of the secondary air in case B encourage us to make further improvement.

4.3. Overlap energy utilization: Case C with CTBO (RC + DRH + RC + DRH + HTC)

The use of RC + DRH (recompression + double-reheating) as the bottom cycle further elevates the average heat absorption temperature for bottom cycle (see Fig. 9). Four heaters are used in bottom cycle, in which Heaters 4a and 4b generate vapor to drive turbine T4, Heater 5 is the first reheating to drive turbine T5, and Heater 6 is the second reheating to drive turbine T6. Among the four heaters, only Heater 4a absorbs moderate flue gas heat, the other three heaters extract high temperature flue gas heat to operate in overlap heating regime. Due to higher CO_2 temperature at the end of T6 (T_{6b}) by using double-reheating, a high temperature cooler (HTC) dissipates extra heat to environment to ensure that case B and case C have the same secondary air temperature. Thus, there are two components of HTC and cooler 2 dissipating extra heat to environment.

The double-reheating in bottom cycle ensures identical vapor temperatures at the inlet of six turbines, three for top cycle and three for bottom cycle, resulting in more components sharing. For example, T4, T5 and T6 in bottom cycle are combined with T1, T2 and T3 in top cycle, respectively. Heaters 5 and 6 are combined with Heaters 2 and 3, respectively. Due to overlap heating and double-reheating in bottom cycle, totally 9 components in bottom cycles are combined with top cycle. It is noted that Heater 4a is a major component to extract moderate flue gas heat, thus Heaters 4a and 4b cannot be combined with other components.

The above cycle layout obviously alters the average heat absorption temperature for bottom cycle, which is increased from 572.0 °C for case B to 591.3 °C for case C, at the main vapor parameters of 700 °C/35 MPa (see Fig. 10). However, a weakness occurs when double-reheating is used for bottom cycle. The high temperature dissipation by HTC apparently changes the average heat release temperature, which is increased from 49.3 °C for case B to 169.9 °C for case C (see Fig. 10). The comprehensive effect of increased average heat absorption temperature $T_{ave,a}$ and release temperature $T_{ave,r}$ deteriorates the thermal efficiency of bottom cycle. At the main vapor parameters of 700 °C/35 MPa, the bottom cycle efficiency $\eta_{th,b}$ is decreased from 53.84% for case B to

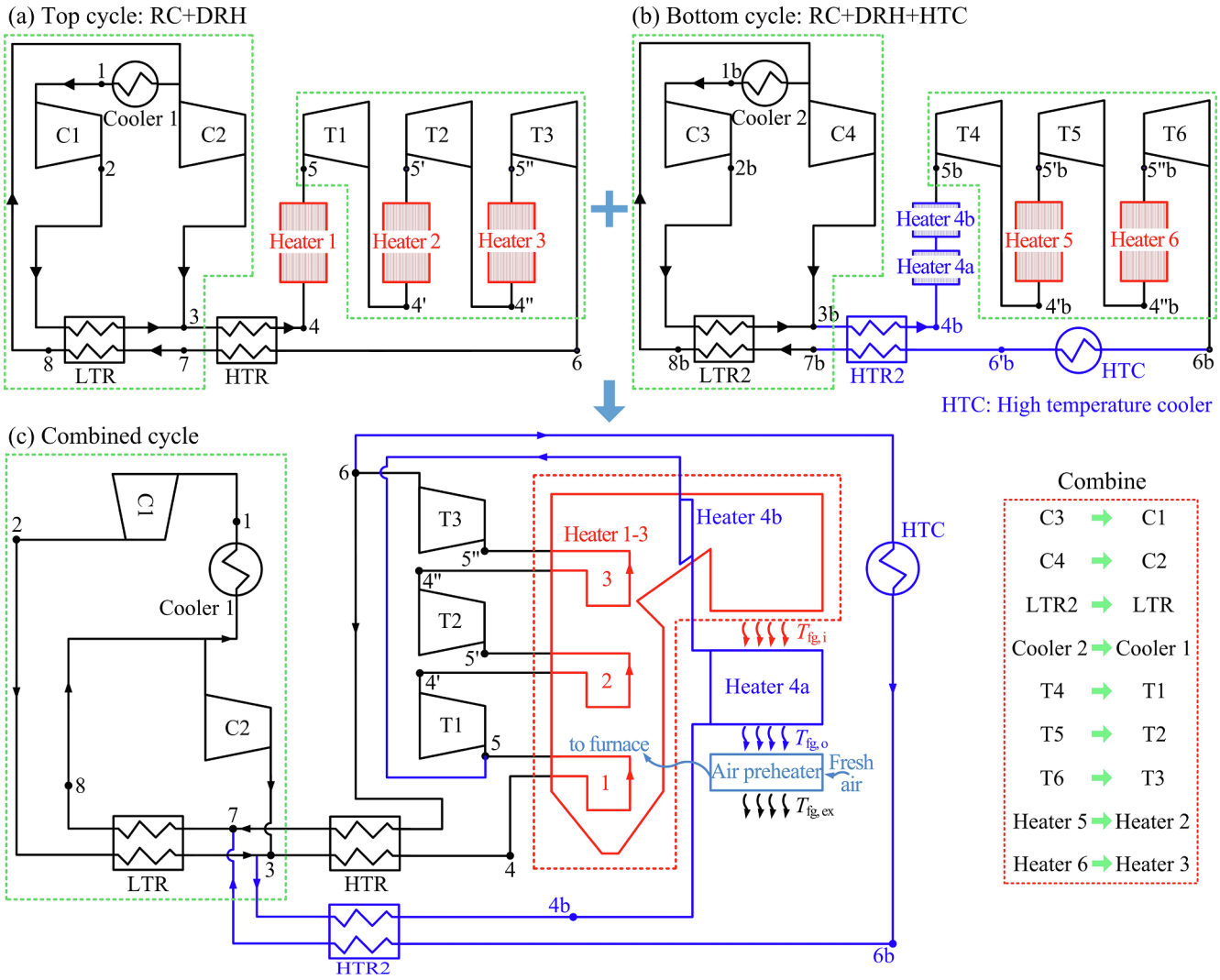

Fig. 9. Case C: CTBO (RC + DRH + RC + DRH + HTC) with overlap absorption of flue gas heat (a: top cycle, b: bottom cycle, c: combined cycle after components sharing).

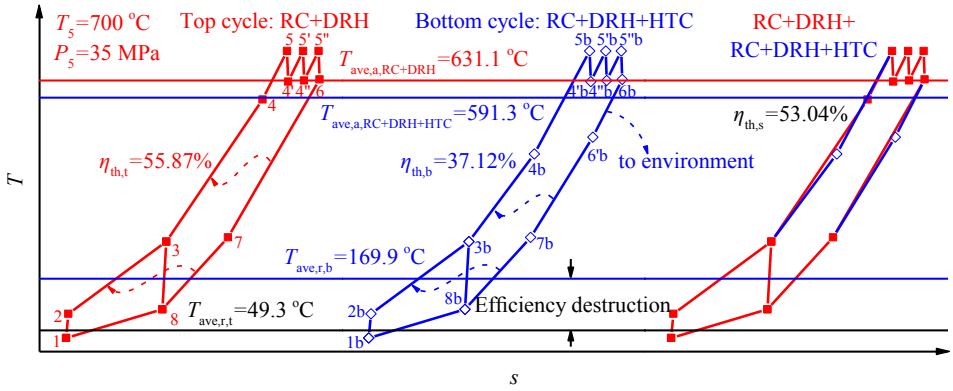

Fig. 10. *T-s* diagram for CTBO (RC + DRH + RC + DRH + HTC): overlap absorption of flue gas heat with constraint of identical vapor temperatures entering and leaving each turbine.

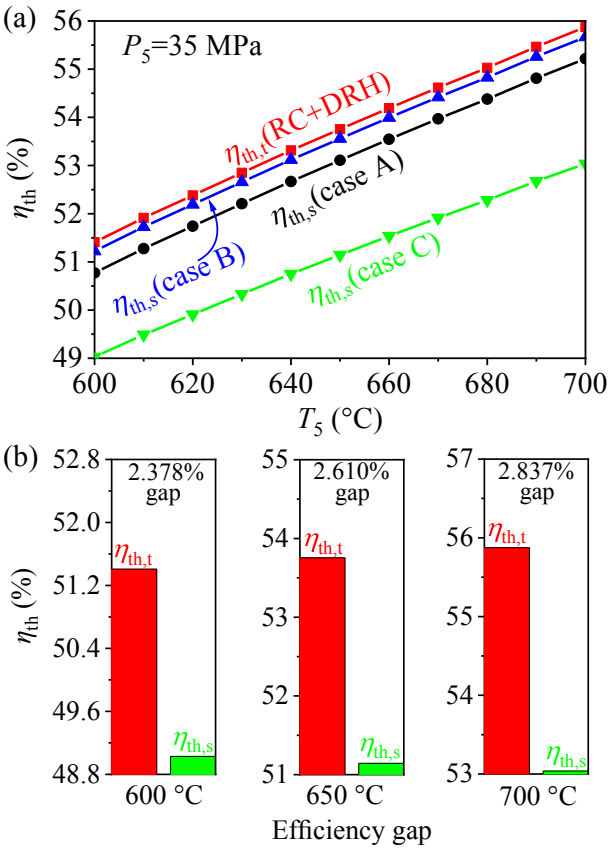

Fig. 11. Thermal efficiencies of cases A, B and C referenced to top cycle RC + DRH (a: efficiencies versus main vapor temperatures, b: efficiency gaps between top cycle and CTBO (RC + DRH + RC + DRH + HTC) at three main vapor temperatures).

37.12% for case C. Correspondingly, Fig. 11 shows that the efficiency gap between the top cycle and the combined cycle for case C attains the range of 2.38%–2.84% adapting the T_5 range of 600–700 °C. It is noted that case C has the highest average heat absorption temperature among cases A, B and C. Our next work is to reduce the average heat release temperature, leading us to reach the maximum efficiency for combined cycle.

4.4. Overlap energy utilization: Case D with CTBO (RC + DRH + RC + DRH + EAP)

For cases A, B and C, there is an air preheater in the boiler tail flue to extract low temperature flue gas heat. The total air flow rate in air preheater is separated into two streams of a primary air and a secondary air. The flue gas heating elevates the two air streams temperatures. Then, the primary air transports coal particles into furnace, while the secondary air directly enters the furnace. Both the two streams are involved in chemical combustion in the furnace.

The air flow chart is modified for case D (see Figs. 12–18). The secondary air after leaving air preheater does not directly enter the furnace. Instead, the air stream is further heated by the extra CO_2 heat of bottom cycle. An additional heat exchanger transfers CO_2 heat to secondary air. Because the heat exchanger heats air in the outside of boiler, it is called external air preheater (EAP). EAP replaces HTC to dissipate extra CO_2 heat to air, not to environment. Thus, the double-reheating induced extra CO_2 heat is recycled into boiler via air.

Fig. 12 shows the cycle layout of case D, in which EAP is marked. In order to understand the effect of EAP on the average heat absorption temperature $T_{ave,a}$ and heat release temperature $T_{ave,r}$ for bottom cycle, Heater 4a in Fig. 9 is decoupled into Heater 4a' and Heater 4a" in Fig. 12. Fig. 13 shows the relationship of thermal loads among air preheater in tail flue, EAP and Heater 4a'. The heat load of EAP is

$$Q_{EAP} = m_{CO_2,b}(h_{6'b} - h_{6b}) \tag{12}$$

where $m_{CO2,b}$ is the CO_2 mass flow rate in bottom cycle, the state point 6′b is at the outlet of turbine T6, 6b is at the outlet of EAP (see Fig. 12). Heater 4a' is decoupled from Heater 4a so that its thermal load equals to Q_{EAP}. The CO_2 fluid in Heater 4a' can be considered as not heated by flue gas, but heated by the recycling heat of EAP.

Fig. 14 shows the *T-s* cycle. There are three heat recycling processes in bottom cycle. The heat load of 6′b6b is recycled to 4b9b via EAP, thus 4b9b is not involved in the calculation of heat absorption temperature. The heat loads of 6b7b and 7b8b are recycled to 3b4b via HTR2 and 2b3b via LTR2, respectively (see Figs. 12 and 14). Due to heat recycling, EAP not only further elevates the average heat absorption temperature $T_{ave,a}$, but also lowers the average heat release temperature $T_{ave,r}$. Referring to Fig. 14, the two temperatures for bottom cycle are

$$T_{ave,a} = \frac{(h_{5b} - h_{9b}) + (h_{5'b} - h_{4'b}) + (h_{5''b} - h_{4''b})}{(s_{5b} - s_{9b}) + (s_{5'b} - s_{4'b}) + (s_{5''b} - s_{4''b})} \tag{13}$$

$$T_{ave,r} = \frac{h_{8b} - h_{1b}}{s_{8b} - s_{1b}} \tag{14}$$

Fig. 14 shows that at the main vapor parameters 700 °C/35 MPa, both top cycle and bottom cycle have identical $T_{ave,a}$ = 631.7 °C and $T_{ave,r}$ = 49.3 °C. Fig. 15 shows that at P_5 = 35 MPa and when T_5 is varied in the range of 600–700 °C, the combined cycle efficiency $\eta_{th,s}$ for case D is exactly equal to the top cycle efficiency $\eta_{th,t}$. Because the bottom cycle repeats the top cycle, the efficiency gap thoroughly disappears, while cases A, B and C cannot do that. The results presented in Fig. 15 is believed to reach maximum thermal efficiency for coal fired power plant. There are two conditions for maximum thermal efficiency. First, both top and bottom cycles use RC + DRH, DRH ensures multi-expansions in turbines in a higher and quasi-uniform temperature level. Second, as an additional heat recycling except HTR and LTR, EAP raises heat absorption temperature and decrease heat release temperature. The repeating of top and bottom cycles is the limit condition to attain the maximum system thermal efficiency.

5. Comments on the overlap energy utilization

Fig. 16 summarizes the roadmap from case A to cases B, C and D, guiding us to obtain the maximum system thermal efficiency. Here, 700 °C/35 MPa is taken as the example of main vapor parameters. In the historical evolution, all the four cases keep the stabilized top cycle having $T_{ave,a}$ = 631.1 °C, $T_{ave,r}$ = 49.3 °C and η_{th} = 55.87%, which are taken as the referenced values to be pursued by bottom cycle using the overlap heating concept.

case A → case B: Case A behaves cascade energy utilization. The

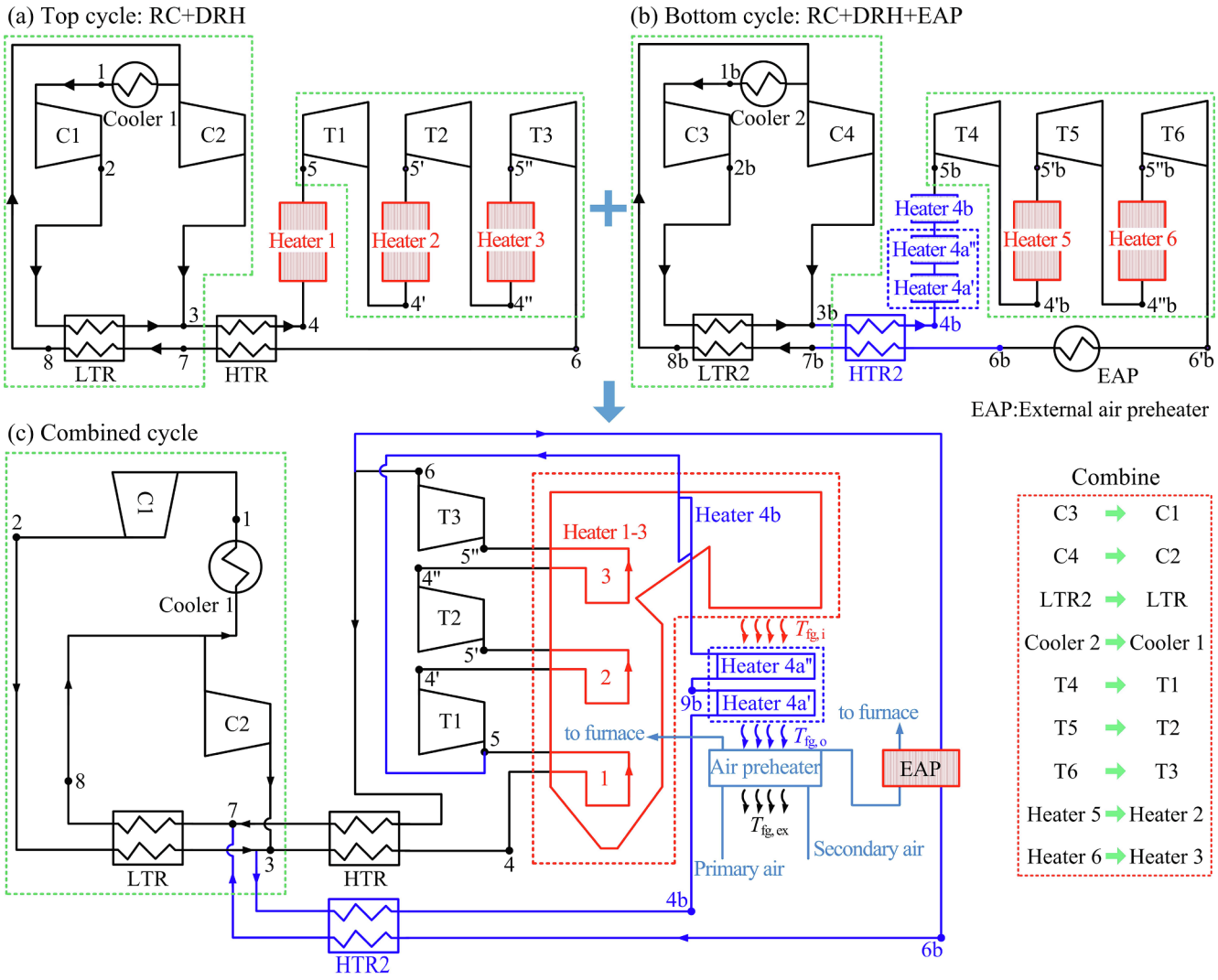

Fig. 12. Case D: CTBO (RC + DRH + RC + DRH + EAP) with overlap absorption of flue gas heat (a: top cycle, b: bottom cycle, c: combined cycle after components sharing).

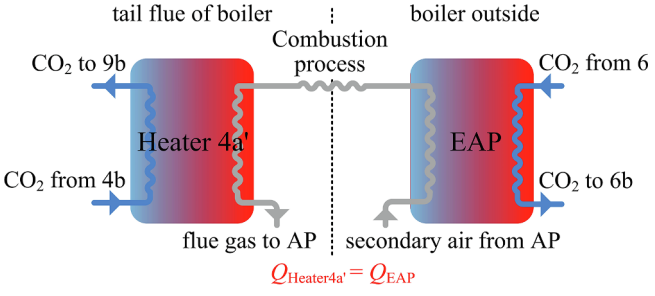

Fig. 13. The heat recycling between EAP and Heater 4a' via air.

bottom cycle has the average heat absorption temperature of 510.4 °C to yield larger efficiency gap between top and bottom cycles. Case B has the same cycle types as case A. Due to overlap energy utilization, the average heat absorption temperature is raised to 572.0 °C for bottom cycle.

case B → case C: Due to overlap energy utilization and double-reheating for bottom cycle, the bottom cycle increases the average heat absorption temperature from 572.0 °C for case B to 591.3 °C for case C. Meanwhile, due to extra CO_2 heat dissipation to environment, the bottom cycle of case C raises the average heat release temperature to 169.9 °C.

case C → case D: To decrease the average heat release temperature for bottom cycle of case C, case D introduces EAP to replace HTC. Due to heat recycling, the bottom cycle repeats the top cycle to reach the maximum system thermal efficiency, noting different CO_2 flow rates for top and bottom cycles.

Fig. 16b shows the system thermal efficiencies to show the largest $\eta_{th,s}$ for case D. As shown in Fig. 16c, the system exergy efficiencies support the distribution of thermal efficiencies among the four cases. It is known that the irreversibility of the whole system and each

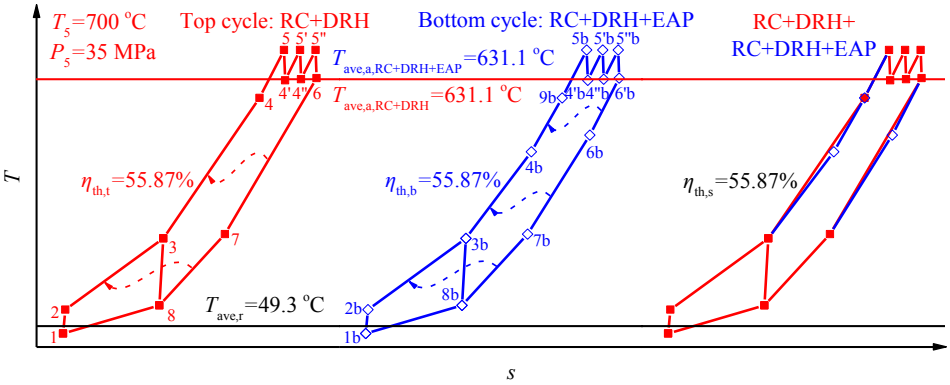

Fig. 14. *T-s* diagram for CTBO (RC + DRH + RC + DRH + EAP): overlap absorption of flue gas heat with constraint of identical vapor temperatures entering and leaving each turbine.

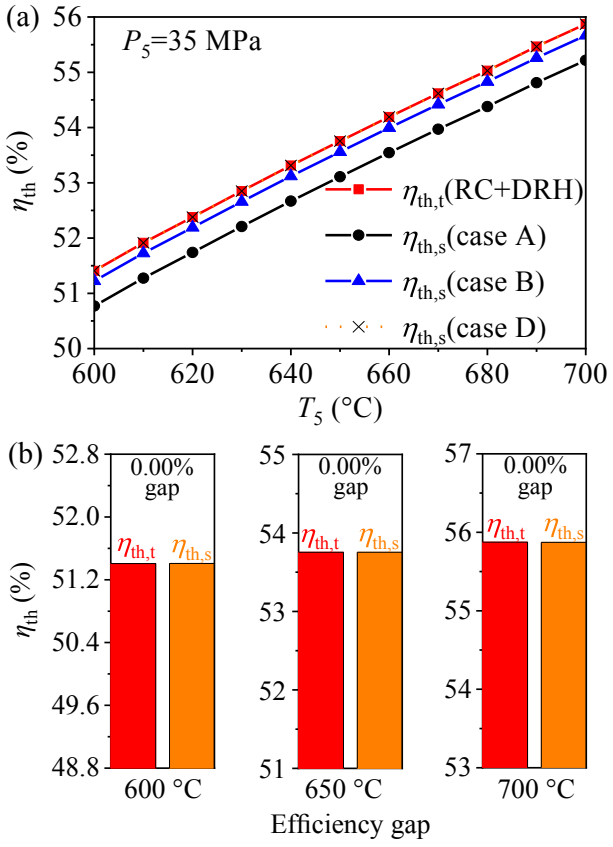

Fig. 15. Thermal efficiencies of cases A, B and D referenced to top cycle RC + DRH, showing no difference between CTBO (RC + DRH + RC + DRH + EAP) and the top cycle of RC + DRH.

component influences the system thermal efficiency. The cycle layout for each case includes boiler, recuperator heat exchanger, cooler, turbine and compressor. For all the four cases, Fig. 17 shows that the S-CO_2 boiler and compressor contribute the largest and smallest exergy destruction in the system, respectively. From case A to case D, the decreased exergy destruction of the boiler is consistent with the raised heat absorption temperature of the cycle. The increased exergy destruction of the cooler in case C accounts for the elevated heat release temperature of the cycle to result in the poor performance of case C.

Fig. 18 shows the S-CO_2 power plant design based on case D. At the main vapor parameters of 620 °C/30 MPa, the power generation efficiency attains 47.99%, which is apparently higher than ~47% for the best water-steam Rankine cycle power plant at the same main vapor parameters. This efficiency improvement creates great energy saving benefit. A 1000 MWe coal fired power plant can save 6.74 tons of standard coal per hour when the efficiency is changed from ~47% to 47.99%.

Fig. 18 is a connected-top-bottom-cycle with overlap heating. Even though the combined cycle is used, the design is simple. Due to recompression (RC), two compressors C1 and C2 are involved. Due to double-reheating, three turbines T1, T2 and T3 are involved. The module design is applied to boiler, significantly reducing pressure drops in boiler tubes. Totally 14 heat transfer modules are coupled with the S-CO_2 cycle. Parts 1–4, SH 1–2, RH 1–4 modules heat CO_2 fluid for top cycle, where SH and RH mean superheater and reheater, respectively. Heaters 4a and 4b heat CO_2 fluid for bottom cycle, absorbing moderate and high temperature flue gas heat, respectively. Heater 4a accounts for a heat load of 128.26 MW, in which 74.3% of the heat load comes from the heat recycling of EAP. For 1000 MWe net power output, the total heat load is 1880.08 MW, including Q_t = 1794.35 MW for top cycle and Q_b = 85.73 MW for bottom cycle, thus $\beta = Q_b/Q_t$ = 4.78% in Eq. (10). The bottom cycle only needs Heater 4a and 4b for heat absorption. Other components such as compressors and turbines are overlapped to top cycle, simplifying the system layout.

The cascade energy utilization was proposed many years ago, which is useful for analysis of various energy systems, such as supercritical steam turbine and combined cycle [3,6], combined system including chemical and physical energies [3,35]. Usually, top cycle and bottom cycle operate in different temperature levels to yield higher top cycle efficiency than bottom cycle. For the present problem, heat transfer temperature difference between flue gas and CO_2 is quite large, especially in high temperature flue gas regime. The cascade energy utilization may completely extract the energy quantity, but causes apparent exergy loss during heat transfer process. The overlap energy utilization not only absorbs moderate temperature flue gas heat, but also deeply

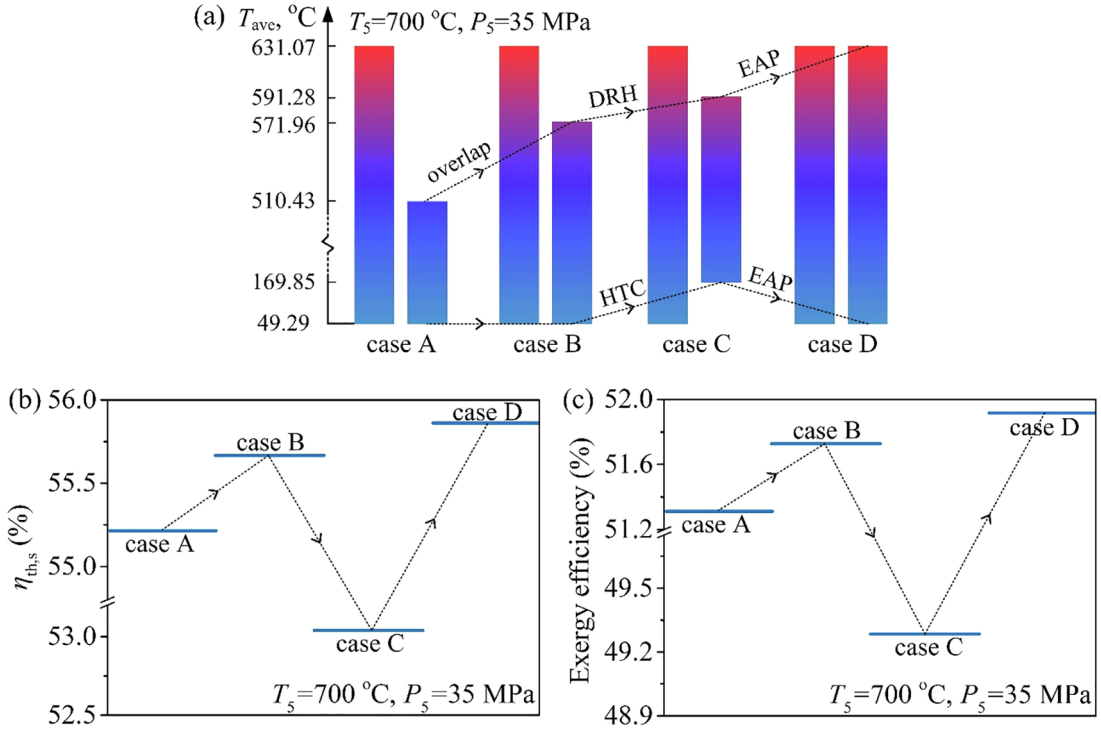

Fig. 16. Roadmap to reach the efficiency limit from A to D.

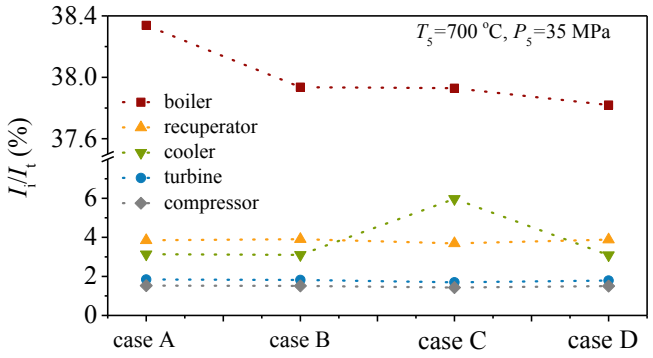

Fig. 17. The exergy destruction of each component to the system (I_t is the total exergy destruction and I_i is the exergy destruction for component *i*).

uses the available exergy of high temperature flue gas. It is expected that the overlap energy utilization can be extended for other energy systems.

6. Conclusions

Cascade energy utilization has been used for various combined cycles. For a coal fired power plant, flue gas covers a very wide temperature range. A single S-CO_2 Brayton cycle cannot extract flue gas heat over entire temperature range. Cascade energy utilization requires a combined cycle. Here, we propose the overlap energy utilization to fill the efficiency gap between top and bottom cycles.

An overlap sub-regime is set in high temperature flue gas regime. Different from cascade energy utilization, top cycle absorbs the most part of high temperature flue gas energy (not all), but bottom cycle not only extracts moderate temperature flue gas heat, but also a fraction of high temperature flue gas heat, thus the average heat absorption temperature of bottom cycle can be apparently raised.

Our numerical simulation supports the above idea. Cases A, B, C and D are analyzed to give a clue to reach maximum efficiency limit of combined cycle. It is believed that case D is the maximum efficiency case, in which both top and bottom cycles use RC + DRH as the cycle type. By using overlap energy utilization and double-reheating, the average heat absorption temperature of bottom cycle is elevated. Because CO_2 temperature at turbine outlet is high due to double-reheating, an external air preheater EAP recycles extra CO_2 heat to system, not to environment. The comprehensive use of overlap energy utilization, double-reheating and EAP repeat top and bottom cycles (noting different mass flow rates of the two cycles), under which the maximum system efficiency is reached. At the main vapor parameters of 700 °C/35 MPa, the thermal efficiency for bottom cycle is increased from 50.89% in case A to 55.87% in case D, showing obvious advantage by using overlap energy utilization compared to cascade energy utilization.

Declaration of Competing Interest

None.

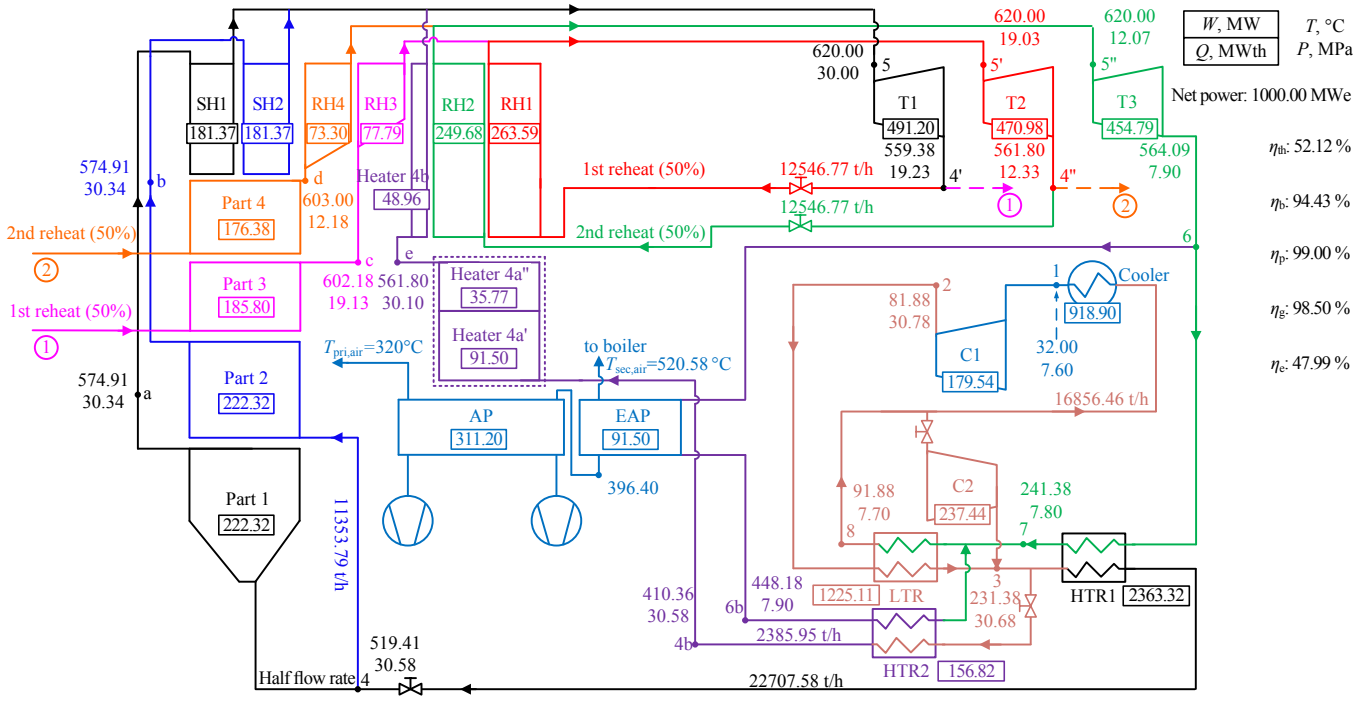

Fig. 18. S-CO_2 coal fired power plant based on case D at the main vapor parameters of 620 °C/30 MPa.

Table 1
S-CO_2 top cycle and air preheater parameters.

Parameters	Values
turbine inlet temperature (T_5)	600–700 °C
turbine inlet pressure (P_5)	35 MPa
turbine isentropic efficiency	93%
compressor C1 inlet temperature (T_1)	32 °C
compressor C1 inlet pressure (P_1)	7.6 MPa
compressors isentropic efficiency	89%
pressure drops in LTR and HTR (ΔP)	0.1 MPa
LTR and HTR pinch temperature difference (ΔT_{LTR} or ΔT_{HTR})	10 °C
primary air temperature	320 °C
primary air temperature at the inlet of air preheater	31 °C
primary air flow rate ratio	19%
secondary air temperature at the inlet of air preheater	23 °C
secondary air flow rate ratio	81%
excess air coefficient	1.2
exit flue gas temperature ($T_{fg,\ ex}$)	123 °C
environment temperature (T_e)	20 °C

Table 2
Parameters for bottom cycle.

Variable/parameter	Value(s)
Turbine isentropic efficiency	93%
Compressor inlet temperature (T_{1b})	32 °C
LP compressor inlet pressure (P_{1b})	7.6 MPa
Compressors isentropic efficiency	89%
Pressure drop of each component except the boiler (ΔP)	0.1 MPa
Pressure drop of the boiler (ΔP_b)	0.2 MPa
LTR2 and HTR2 pinch temperature difference (ΔT_{LTR2} or ΔT_{HTR2})	10 °C

Table 3
Properties of the designed coal.

C_{ar}	H_{ar}	O_{ar}	N_{ar}	S_{ar}	A_{ar}	M_{ar}	V_{daf}	Q_f
61.70	3.67	8.56	1.12	0.60	8.80	15.55	34.73	23,442

C (carbon), *H* (hydrogen), *O* (oxygen), *N* (nitrogen), *S* (sulfur), *A* (ash), *M* (moisture), *V* (Volatile).
Subscripts *ar*, *daf* means as received, dry and ash free, $C_{ar} + H_{ar} + O_{ar} + N_{ar} + S_{ar} + A_{ar} + M_{ar} = 100$.
Q_f means low heat value of coal (kJ/kg).

Acknowledgements

The study was supported by the National Key R&D Program of China (2017YFB0601801), and the Natural Science Foundation of China (51821004).

References

[1] Parsons RH. The early days of the power station industry. Cambridge: Cambridge University Press; 2015.
[2] Xu C, Bai P, Xin T, Hu Y, Xu G, Yang Y. A novel solar energy integrated low-rank coal fired power generation using coal pre-drying and an absorption heat pump. Appl Energ 2017;200:170–9.
[3] Zhang G, Zheng J, Yang Y, Liu W. Thermodynamic performance simulation and concise formulas for triple-pressure reheat HRSG of gas-steam combined cycle under off-design condition. Energ Convers Manage 2016;122:372–85.
[4] Al-Zareer M, Dincer I, Rosen MA. Development and assessment of a novel integrated nuclear plant for electricity and hydrogen production. Energ Convers Manage 2017;134:221–34.
[5] Reddy VS, Kaushik SC, Tyagi SK. Exergetic analysis and performance evaluation of parabolic trough concentrating solar thermal power plant (PTCSTPP). Energy 2012;39:258–73.
[6] Tumanovskii AG, Shvarts AL, Somova EV, Verbovetskii EK, Avrutskii GD, Ermakova SV, et al. Review of the coal-fired, over-supercritical and ultra-supercritical steam

power plants. Therm Eng 2017;64:83–96.
[7] Zhang N, Zhu Z, Yue G, Jiang D, Xu H. The oxidation behaviour of an austenitic steel in deaerated supercritical water at 600–700 °C. Mater Charact 2017;132:119–25.
[8] Sarrade S, Féron D, Rouillard F, Perrin S, Robin R, Ruiz J, et al. Overview on corrosion in supercritical fluids. J Supercritical Fluids 2017;120:335–44.
[9] Sulzer G. Verfahren zur Erzeugung von Arbeit aus Warme. Swiss Patent 1950. 269599.
[10] Feher EG. The supercritical thermodynamic power cycle. Energy Convers 1968;8:85–90.
[11] Angelino G. Carbon dioxide condensation cycles for power production. J Eng Power 1968;90:287–95.
[12] Holcomb GR, Carney C, Doğan ÖN. Oxidation of alloys for energy applications in supercritical CO_2 and H_2O. Corros Sci 2016;109:22–35.
[13] Dostal V. A supercritical carbon dioxide cycle for next generation nuclear reactors [PhD thesis]. Massachusetts Inst Technol2004.
[14] Linares JI, Cantizano A, Arenas E, Moratilla BY, Martín-Palacios V, Batet L. Recuperated versus single-recuperator re-compressed supercritical CO_2 Brayton power cycles for DEMO fusion reactor based on dual coolant lithium lead blanket. Energy 2017;140:307–17.
[15] Moisseytsev A, Sienicki JJ. Investigation of alternative layouts for the supercritical carbon dioxide Brayton cycle for a sodium-cooled fast reactor. Nucl Eng Des 2009;239:1362–71.
[16] Wang X, Liu Q, Lei J, Han W, Jin H. Investigation of thermodynamic performances for two-stage recompression supercritical CO_2 Brayton cycle with high temperature thermal energy storage system. Energ Convers Manage 2018;165:477–87.
[17] Wang K, He Y. Thermodynamic analysis and optimization of a molten salt solar power tower integrated with a recompression supercritical CO_2 Brayton cycle based on integrated modeling. Energ Convers Manage 2017;135:336–50.
[18] Si N, Zhao Z, Su S, Han P, Sun Z, Xu J, et al. Exergy analysis of a 1000 MW double reheat ultra-supercritical power plant. Energ Convers Manage 2017;147:155–65.
[19] Zhao Y, Wang S, Duan L, Lei Y, Cao P, Hao J. Primary air pollutant emissions of coal-fired power plants in China: current status and future prediction. Atmos Environ 2008;42:8442–52.
[20] Fan C, Pei D, Wei H. A novel cascade energy utilization to improve efficiency of double reheat cycle. Energ Convers Manage 2018;171:1388–96.
[21] Notton G, Nivet M, Voyant C, Paoli C, Darras C, Motte F, et al. Intermittent and stochastic character of renewable energy sources: consequences, cost of intermittence and benefit of forecasting. Renew Sustain Energy Rev 2018;87:96–105.
[22] Merzic A, Music M, Haznadar Z. Conceptualizing sustainable development of conventional power systems in developing countries-A contribution towards low carbon future. Energy 2017;126:112–23.
[23] Singh R, Miller SA, Rowlands AS, Jacobs PA. Dynamic characteristics of a direct-heated supercritical carbon-dioxide Brayton cycle in a solar thermal power plant. Energy 2013;50:194–204.
[24] Baik S, Kim SG, Lee J, Lee JI. Study on CO_2-water printed circuit heat exchanger performance operating under various CO_2 phases for S-CO_2 power cycle application. Appl Therm Eng 2017;113:1536–46.
[25] Xu J, Sun E, Li M, Liu H, Zhu B. Key issues and solution strategies for supercritical carbon dioxide coal fired power plant. Energy 2018;157:227–46.
[26] Sun E, Xu J, Li M, Liu G, Zhu B. Connected-top-bottom-cycle to cascade utilize flue gas heat for supercritical carbon dioxide coal fired power plant. Energ Convers Manage 2018;172:138–54.
[27] Mecheri M, Le Moullec Y. Supercritical CO_2 Brayton cycles for coal-fired power plants. Energy 2016;103:758–71.
[28] Park S, Kim J, Yoon M, Rhim D, Yeom C. Thermodynamic and economic investigation of coal-fired power plant combined with various supercritical CO_2 Brayton power cycle. Appl Therm Eng 2018;130:611–23.
[29] Bejan A. Advanced engineering thermodynamics. New York: John Wiley & Sons; 2016.
[30] Chen D. Power cycle analysis. Shanghai: Shanghai Science Press; 1983. [in Chinese].
[31] Sarkar J. Second law analysis of supercritical CO_2 recompression Brayton cycle. Energy 2009;34:1172–8.
[32] Li QD, Liu ZZ. Thermal economy calculation and analysis of thermal power plant. Beijing: China Electric Power Press; 2008. [in Chinese].
[33] Hanak DP, Manovic V. Calcium looping with supercritical CO_2 cycle for decarbonisation of coal-fired power plant. Energy 2016;102:343–53.
[34] Wang L, Deng L, Tang C, Fan Q, Wang C, Che D. Thermal deformation prediction based on the temperature distribution of the rotor in rotary air-preheater. Appl Therm Eng 2015;90:478–88.
[35] Jin H, Ishida M. Reactivity study on a novel hydrogen fueled chemical-looping combustion. Int J Hydrogen Energ 2001;26:889–94.